Electromechanical Properties of Metallic, Quasimetallic, and Semiconducting Carbon Nanotubes under Stretching

Jien Cao, Qian Wang, and Hongjie Dai*

Department of Chemistry, Stanford University, Stanford, California 94305

(Received 11 November 2002; published 18 April 2003)

An electromechanical system is constructed to explore the electrical properties of various types of suspended single-walled carbon nanotubes under the influence of tensile stretching. Small band-gap semiconducting (or quasimetallic) nanotubes exhibit the largest resistance changes and piezoresistive gauge factors ($\sim$ 600 to 1000) under axial strains. Metallic nanotubes exhibit much weaker but nonzero sensitivity. Comparison between experiments and theoretical predictions and potential applications of nanotube electromechanical systems for physical sensors (e.g., strain gauges, pressure sensors, etc.) are discussed.

DOI: 10.1103/PhysRevLett.90.157601 PACS numbers: 77.65.–j, 73.22.–f, 73.63.–b, 77.84.–s

Single-walled carbon nanotubes (SWNTs) are ideally suited for investigating the electrical, mechanical, and electromechanical (EM) properties of molecular materials [1]. An interesting subject has been how bond stretching and twisting in nanotubes affect the electrical properties of nanotubes. An appreciable body of theoretical literature exists [2–12] on this topic, but only one experimental work [13] has been published thus far. In general, theory has suggested that the electromechanical properties of SWNTs depend on nanotube chirality defined by the tube index (m, n) [2,3,7,8,10]. Armchair metallic SWNTs (M-SWNT, $m = n$) retain their high symmetry under tensile stretching and the electrical properties should be the least sensitive to tensile strain. Other types of SWNTs with lower symmetries, including quasimetallic (or small band-gap semiconducting, SGS-SWNT, $m - n = 3N$, $N =$ integer) and semiconducting nanotubes (S-SWNT, $m - n \neq 3N$) are more sensitive and can exhibit band-gap changes under tensile stretching [2,3,7,8,10].

Experimentally, Tombler *et al.* used atomic force microscope (AFM) tips to push suspended SWNTs and observed up to 2 orders of magnitude conductance change at high strains ($\sim$3%) for metallic SWNTs [13]. Theoretical simulation and conductance calculations for true metallic armchair (5,5) tubes suggested that the drastic conductance decrease was associated with large local deformation [9,13]. Uniform axial strain in metal tubes was insufficient to turn them into a nearly insulating state. Maiti *et al.* suggested from simulation results that, if the SWNT was quasimetallic of, e.g., (12,0) chirality, then uniform axial strain could explain the experimental result due to band-gap opening [11,12].

Here, we investigate the EM properties of suspended M-, SGS-, and S-SWNTs in a device geometry that allows for more uniform tensile stretching of nanotubes, without direct nanotube pushing by sharp tips. The basic device structure consists of individual SWNTs suspended over micromechanical poly-silicon cantilevers (1 μm thick, 30 μm long, and 5 μm wide) and solid terraces (Fig. 1). The device fabrication and SWNT integration are done in arrayed fashion as reported previously [14], involving premade molybdenum electrodes on both the cantilevers and the terraces and subsequent patterned growth of SWNTs to physically and electrically bridge the elevated structures (Fig. 1). The Si substrate acts as a functional gate for the suspended nanotubes, albeit with a low efficiency due to the $\sim$2 μm distance and the existence of an air gap [Fig. 1(b)]. For electromechanical measurement, we use an AFM tip (AFM cantilever spring constant $\sim$40 N/m) to push the free end of the poly-Si beam (spring constant $\sim$8 N/m). The downward bending of the beam toggles on the suspended nanotube, causing nanotube stretching [Fig. 1(c)]. The electrical conductance of the nanotube and beam deflection are monitored in real time (referred to as EM data). Afterwards, we perform scanning electron microscope (SEM) imaging of the sample (with 10 nm evaporated Au to avoid charging) to ensure that individual SWNTs are bridging the measured devices [Fig. 1(b)].

Figure 2(b) shows the raw EM data obtained with an SGS-SWNT over repeated stretching. The nanotube exhibits small band-gap [2,15–17] characteristics with a dip [15] in the conductance (G) vs gate (V_g) characteristics [Fig. 2(a)]. The poly-Si beam deflection (δZ_{beam}) and nanotube conductance vs the vertical coordinate Z for one pushing cycle are shown in the top and bottom panels of Fig. 2(c), respectively. The initial point of contact between the AFM tip and the poly-Si beam on the sample is defined as Z_0. The deflection of the beam (δZ_{beam}) is then related to the AFM cantilever deflection δZ_{AFM} through $\delta Z_{\text{beam}} = (Z - Z_0) - \delta Z_{\text{AFM}}$. That is, the total sample stage movement after the Z_0 point equals the sum of the deflections of the poly-Si beam and the AFM cantilever. With SEM, we often find varying degrees of slack in the suspended SWNTs. This is consistent with EM data that the conductance of the SWNTs does not exhibit an immediate change after the initial Z_0 contact

point. Additional pushing is needed to straighten and stretch the nanotube. The strain σ is calculated by

$$\sigma = (L_T' - L_T)/L_T = \sqrt{L_T^2 + (\delta Z^0_{\text{beam}} + \delta Z^1_{\text{beam}})^2}/\sqrt{L_T^2 + (\delta Z^0_{\text{beam}})^2} - 1, \quad (1)$$

where L_T is the length of the SWNT if no slack existed, δZ^0_{beam} is the beam deflection needed to straighten the nanotube, and δZ^1_{beam} is the additional beam deflection pushed by the AFM tip after the straightening point.

For small strains ($< 1\%$), we find the conductance of suspended SWNTs highly reversible upon repeated stretching and releasing [Fig. 2(b)]. This suggests that the contacts between the nanotube and metal electrodes are not irreversibly changed during repeated nanotube stretching and relaxing. Further pushing beyond 1% strain tends to cause irreversible changes to the device conductance, presumably due to nanotube lifting off from the end of the cantilever surface as it is pushed significantly downward by the AFM tip. The conductance of the SGS-SWNT device in Fig. 2(b) decreases by about 1 order of magnitude at the maximum strain point and is highly reversible over repeated pushing cycles. The initial resistance of the device (under $V_g = 0$ used during stretching) is $R_0 \sim 250$ kΩ. With the strain analysis described above ($\delta Z^0_{\text{beam}} \sim 330$ nm suggesting a slack of $\sim$21 nm in tube suspension; slack revealed by SEM $\sim$17 nm), we obtain a normalized resistance change ($\delta R/R_0$) vs strain σ curve [Fig. 2(d)]. The resistance increases nearly linearly for small strains ($\sigma < 0.2\%$), and increases more significantly at higher strains. Data analysis for repeated pushing cycles yields highly reproducible ($\delta R/R_0$) vs σ results [nearly overlapping curves in Fig. 2(d)]. The piezoresistive gauge factor for the SGS-SWNT defined as $\beta_{\text{GF}} = (\delta R/R_0)/\sigma$ is about 600 for $\sigma < 0.2\%$ ($\delta R = 220$ kΩ for $\sigma = 0.15\%$). We have systematically measured and analyzed two SGS-SWNT devices ($R_0 \sim 300$ kΩ for the second device), and obtained gauge

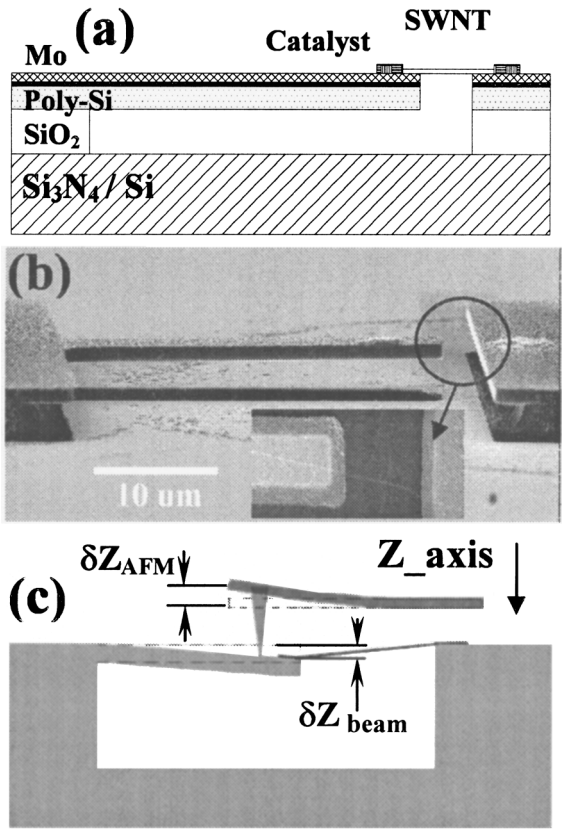

FIG. 1. (a) A schematic device structure. The device fabrication started with a p-type Si with a 200 nm-thick thermally grown oxide. A Si_3N_4 (200 nm-thick, HF etch-stop for beam release), SiO_2 (2 μm thick by low pressure chemical vapor deposition, sacrificial layer for cantilever release), poly-Si (1 μm, for cantilever beam), Si_3N_4 (10 nm layer separating Mo from poly-Si), and Mo (50 nm) films were successively deposited, before catalyst patterning, defining the shapes of cantilevers and terraces by photolithography, cantilever release, and SWNT growth. (b) An SEM image of a device. Inset: Zoom-in view of a suspended SWNT. (c) Scheme for stretching a nanotube.

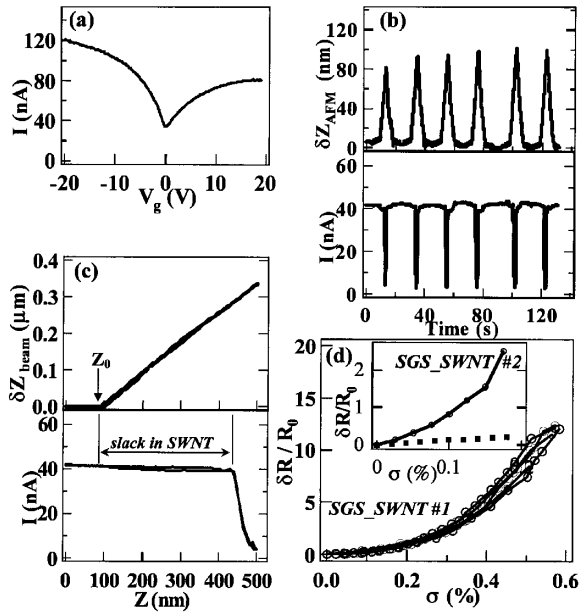

FIG. 2. (a) I-V_g characteristics for an SGS-SWNT. (b) Real time data of AFM cantilever deflection (top panel) and current (bottom) through the SWNT (under bias = 10 mV) during multiple manipulation cycles. (c) Beam deflection (top) vs Z and current (bottom panel, bias = 10 mV) vs Z for one cycle. (d) Normalized resistance change vs strain for the nanotube. Inset: Data for another SGS-SWNT. Lines are drawn to guide the eye in ($\delta R/R_0$)-σ plots. The solid squares are calculated data points based on the band-gap change theory described in the text. Note that the data shown here were representative of $\sim$5 SGS tube devices. On occasion, we observed conductance increase under strain with a device. This could be consistent with the prediction of narrowing of E_g for certain types of SWNTs under strain [7,8,10]. Nevertheless, this behavior is rare and needs to be reproduced with more samples.

factors of $600 \sim 1000$. The Fig. 2(d) inset shows the $(\delta R/R_0)$ vs σ data for the second SGS-SWNT device with $\beta_{GF} = (\delta R/R_0)/\sigma \sim 1000$ ($\delta R = 450\ \mathrm{k}\Omega$ for $\sigma = 0.15\%$). Importantly, we have measured the slacks in all of our suspended-SWNT devices by direct SEM imaging. Correlating with EM data ($\delta Z^0_{\mathrm{beam}}$ values), we find that changes in conductance of all of our devices become measurable right after the straightening point of the slacked SWNTs.

Figure 3 shows the electromechanical data for a semiconducting SWNT. The I-V_g characteristics of this tube exhibit 4 orders of magnitude change by gate voltages [Fig. 3(a) inset] and appears like a p-type field effect transistor (FET). Since the semiconducting SWNT device is normally OFF at $V_g = 0$, we carried out stretching measurement at $V_g = -20$ V under which $R_0 \sim 300\ \mathrm{k}\Omega$. A gauge factor of $\beta_{GF} = (\delta R/R_0)/\sigma \sim 150$ is found for the S-SWNT device in the linear region of $(\delta R/R_0)$ vs σ [Fig. 3(b), $\delta R = 70\ \mathrm{k}\Omega$ for $\sigma = 0.15\%$].

Figure 4 shows the data for a metallic M-SWNT device that exhibits no conductance vs gate-voltage dependence [Fig. 4(a) inset]. The initial resistance of the suspended-SWNT (slack ~80 nm measured from both SEM and EM data) device is ~140 kΩ. From $(\delta R/R_0)$ vs σ [Fig. 4(b)], we obtain $\beta_{GF} = (\delta R/R_0)/\sigma \sim 40$ ($\delta R = 8.3\ \mathrm{k}\Omega$ for $\sigma = 0.15\%$). Measurements and analyses over two M-SWNTs yield β_{GF} on the order of 40–60. $(\delta R/R_0)$ vs σ for the second M-SWNT with $\beta_{GF} \sim 60$ is shown in the Fig. 4(b) inset.

A definitive trend of $\beta_{GF}(\text{SGS-SWNTs}) > \beta_{GF}(\text{S-SWNTs}) > \beta_{GF}(\text{metallic SWNTs})$ is thus observed in our experiments. Larger absolute resistance changes have also been measured for SGS-SWNTs (under the same strain of $\sigma = 0.15\%$, the resistance changes for SGS- and M-SWNTs are $\delta R \sim 400\ \mathrm{k}\Omega$ and ~8 kΩ, respectively). To compare our experimental results with theory, we note that theoretical predictions on the effect of uniform strain to the electrical properties of SWNTs have mostly focused on band-gap changes [2,3,7,8,10]. Within the framework of tight binding (TB) without σ-π orbital coupling (or curvature effects), Yang *et al.* have derived the band-gap change for metallic and semiconducting SWNTs [10],

$$|dE_g/d\sigma| = 3t_0(1 + \nu)\sin 3\alpha, \tag{2}$$

where $t_0 = 2.66$ eV is the hopping integral in the Hamiltonian for nearest-neighbor atoms, $\nu = 0.2$ is the Poisson's ratio for nanotubes, and α is the chiral angle. Kleiner and Eggert derived the band-gap evolution for quasimetallic SWNTs under strain σ [8],

$$E_g = \left| \left(\frac{\gamma a^2}{16R^2} - \frac{ab\sqrt{3}}{2}\sigma \right) \sin 3\alpha \right|, \qquad |dE_g/d\sigma| = \frac{ab\sqrt{3}}{2}\sin 3\alpha, \tag{3}$$

where $a = 2.5$ Å is the graphene Bravais lattice vector, R

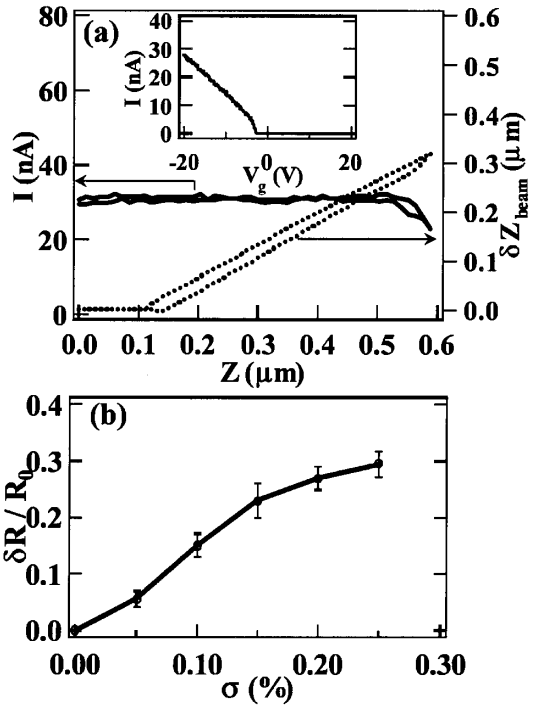

FIG. 3. (a) EM data for a S-SWNT. Inset: FET-like I-V_g characteristics. Bias voltage = 10 mV. (b) Normalized resistance change vs strain recorded under $V_g = -20$ V.

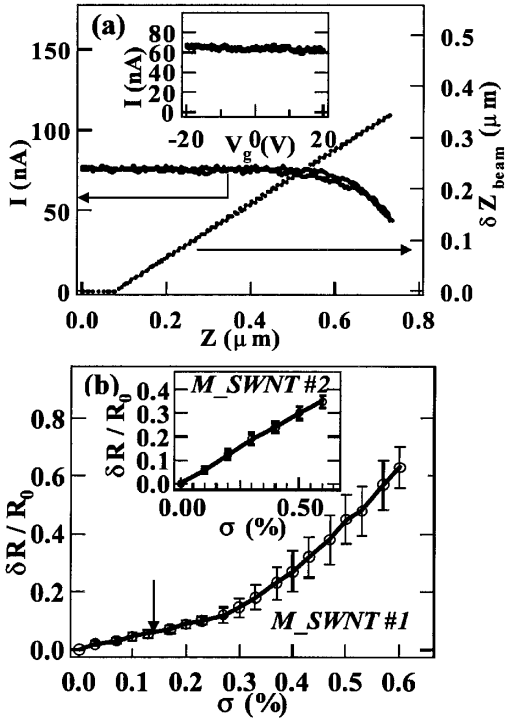

FIG. 4. (a) EM data for a M-SWNT. Inset: I-V_g characteristics. Bias voltage = 10 mV. (b) Normalized resistance change vs strain for the M-SWNT. Inset: Data for another M-SWNT.

is the tube radius, and $b = 3.5$ eV/Å is the linear change in hopping integral vs bond length change.

Among all chirality SWNTs, armchair tubes are predicted to be the most insensitive to tensile deformation with no band-gap opening [$\Delta E_g = 0$, $\alpha = 0$, Eq. (2)] under tensile strain. This is qualitatively in agreement with the trend observed experimentally. Equations (2) and (3) predict band-gap changes for semiconducting and quasimetallic SWNTs under a small strain of 0.1% (~ 1 GPa stress) are $(9.3 \sin 3a)$ meV and $(7.6 \sin 3a)$ meV, respectively, with zigzag tubes ($\alpha = \pi/6$) exhibiting the largest change for both types of SWNTs. The largest band-gap changes predicted for semiconducting and quasimetallic SWNTs are similar, up to $\sim$10 meV for $\sigma = 0.1\%$ strain. Since E_g are $\sim$0.5 eV and in the meV range for undeformed S-SWNT and SGS-SWNT, respectively, a similar band-gap change of $\Delta E_g \sim 10$ meV should cause a larger electrical resistance change to SGS-SWNTs than to S-SWNTs. This is in qualitative agreement with our experimental results. However, quantitatively, our analysis suggests that the band-gap change scenario cannot fully account for the experimental EM results. For SGS-SWNTs, we have modeled $R(\sigma) \approx R_c + R'\{1 + \exp[E_g(\sigma)/2KT]\}$, where R_c is the contact resistance and R' is a prefactor on the order of quantum resistance (thermal activation through a $E_g/2$ barrier has been observed previously in temperature dependent measurements of SGS-SWNT) [15], and found that, for $\delta R(\sigma)/R \sim 1$, a band-gap widening by 45 meV is needed. This requires $\sigma > 0.5\%$ according to Eq. (3), which is a factor of 5 higher than the experimentally observed strain of $\sigma \sim 0.1\%$ under which $\delta R(\sigma)/R \sim 1$ [Fig. 2(d) inset]. That is, the experimentally measured $\delta R(\sigma)/R$ is larger than that caused by strain induced band-gap changes [Fig. 2(d) inset, solid squares].

The resistance changes for both metallic ($\delta R \sim 1.2 R_Q$ at $\sigma = 0.15\%$, $R_Q = h/4e^2 = 6.5$ kΩ) and quasimetallic ($\delta R \sim 60 R_Q$) tubes are larger than expected by band-gap theories, suggesting that other electromechanical effects and mechanisms may operate in our devices. These effects are currently not understood and require further experimental and theoretical investigation. We cannot completely rule out the effects of larger local tube deformations at the edges of the suspended beams and terraces as the precise sharpness of these structures is difficult to characterize. Nevertheless, for the small strains involved here, it is not likely that sharp bending or kinks exist at the edges in the suspended SWNTs. We also point out that the resistances of our current Mo-contacted SWNTs (in unstretched states) are relatively high ($R_0 \sim$ 100–300 kΩ for SGS-SWNTs and M-SWNTs). This is mainly caused by high contact resistance likely to be associated with slight oxidation of the Mo electrodes in the ambient. As a comparison, Ti/Au contacted SWNTs (nonsuspended, with metal covering nanotube) grown by the same growth process always exhibit lower resistance ($R_0 =$ 10–100 kΩ) [15,18,19]. More ideally contacted suspended-SWNT devices with R_0 near the quantum resistance $R_Q = h/4e^2 = 6.5$ kΩ are desired for elucidating the intrinsic gauge factors of SWNTs.

In summary, we have carried out a systematic investigation of the electromechanical properties of various types of SWNTs under tensile strain. In the small strain range, quasimetallic nanotubes exhibit the highest sensitivity to tensile stretching (β_{GF} up to 600–1000) while metallic nanotubes are the least sensitive, in qualitative agreement with existing theoretical expectations. The result suggests that, at room temperature, quasimetallic SWNTs are potentially useful for highly sensitive eletromechanical sensors and could present a new type of strain gauge material (conventional doped-Si strain gauges have $\beta_{GF} \sim 200$) [20]. Further work is needed to fully understand the basic EM properties of various types of SWNTs. Also, we are currently replacing Mo with more transparent metal contacts and devising new strategies to deform nanotubes.

We thank Professor S.-Y. Wu for useful discussions. This work is supported by an NSF-NIRT, MARCO MSD Focus Center, ABB Group Ltd., and the Packard, Sloan and Camille Henry Dreyfus Foundations.

*Email address: hdai@stanford.edu

[1] M. S. Dresselhaus, G. Dresselhaus, and P. Avouris, in *Carbon Nanotubes* (Springer-Verlag, Berlin, 2001), Vol. 80.
[2] C. L. Kane and E. J. Mele, Phys. Rev. Lett. **78**, 1932 (1997).
[3] R. Heyd, A. Charlier, and E. McRae, Phys. Rev. B **55**, 6820 (1997).
[4] M. Nardelli and J. Bernholc, Phys. Rev. B **60**, R16 338 (1999).
[5] A. Rochefort, D. Salahub, and P. Avouris, Chem. Phys. Lett. **297**, 45 (1998).
[6] A. Rochefort *et al.*, Phys. Rev. B **60**, 13 824 (1999).
[7] L. Yang *et al.*, Phys. Rev. B **60**, 13 874 (1999).
[8] A. Kleiner and S. Eggert, Phys. Rev. B **63**, 073408 (2001).
[9] L. Liu *et al.*, Phys. Rev. Lett. **84**, 4950 (2000).
[10] L. Yang and J. Han, Phys. Rev. Lett. **85**, 154 (2000).
[11] A. Maiti, Chem. Phys. Lett. **331**, 21 (2000).
[12] A. Maiti, A. Svizhenko, and M. P. Anantram, Phys. Rev. Lett. **88**, 126805 (2002).
[13] T. Tombler *et al.*, Nature (London) **405**, 769 (2000).
[14] N. R. Franklin *et al.*, Appl. Phys. Lett. **81**, 913 (2002).
[15] C. Zhou, J. Kong, and H. Dai, Phys. Rev. Lett. **84**, 5604 (2000).
[16] M. Ouyang *et al.*, Science **292**, 702 (2001).
[17] M. E. Itkis *et al.*, Nano Lett. **2**, 155 (2002).
[18] H. Soh *et al.*, Appl. Phys. Lett. **75**, 627 (1999).
[19] J. Kong *et al.*, Phys. Rev. Lett. **87**, 106801 (2001).
[20] J. Fraden, *Handbook of Modern Sensors* (Springer-Verlag, New York, 1996).